第 48 卷 第 6 期
2021 年 6 月

湖南大学学报（自然科学版）
Journal of Hunan University（Natural Sciences）

Vol. 48. No. 6.
June 2021

Influence of Geomorphology and Siltstone Structure on the Land Vulnerability in Mamberamo Raya, Papua, Indonesia

Adi Tonggiroh*

Department of Geology, Hasanuddin University, Makassar, South Sulawesi 90245, Indonesia

Abstract: Mamberamo Raya is one of the most prone areas in Papua, Indonesia, due to frequent earthquakes. The researchers analyzed the relationship between the pattern and direction of the fault-stress structure and geochemical characteristics of siltstone on land vulnerability. The fault structure and land vulnerability pattern and direction were analyzed from the direct interpretation of the Digital Elevation Model map, outcrop descriptions, petrography, stereology, rainfall classification, earthquake estimation curves, landslide data. Siltstone geochemical characteristics were collected from selected rock outcrops that were outside the fault structure area. In each location, claystone, sandstone, and siltstone samples were collected before identifying at the Optical Mineral Laboratory in the Department of Geology, Hasanuddin University. The pattern and direction of the fault-stress structure and the siltstone geochemical characteristics affected the land vulnerability. The trend of seismic activity was highly associated with regional-scale faults, such as the fold and thrust fault belt of Guinea, Gauttier-Roufaer Central Range fault, Sarmi fault, Waropen fault, and Mamberamo fault. The earthquake dynamics that affected the southern part of the local-scale fault area were overlapped with an area of stripped rock with the shear plane. There were alternating sandstone, greywacke, claystone, and siltstone layers with chemical compositions of Al, Ca, Fe, K, and Mg and the age of the rock formation. The shear plane vulnerability may cause soil erosion and unstable slopes. Based on the mapping results, the areas with extremely high vulnerability were found in northeast Anggreso, north of Pioneer Birak, and the southwest of Kasonaweja. Moreover, high-vulnerability areas are also detected on the hillsides south of Burmeso, while the land vulnerability in Kanonaweja and Burmeso was classified as medium or low. The outcrop existence and stripped rock with shear plane highly influence the silt-stone structure on the land susceptibility in the studied area.

Keywords: fault-stress structure, land, vulnerability, geochemical characteristics, Mamberamo Raya.

印度尼西亚巴布亚曼巴莫开斋节 地貌和粉砂岩结构对土地脆弱性的影响

摘要：由于频繁发生地震，曼巴莫开斋节是印度尼西亚巴布亚最容易发生地震的地区之一。研究人员分析了断层应力结构的模式和方向与粉砂岩地球化学特征对陆地脆弱性的关系。从数字高程模型图的直接解释、露头描述、岩相学、立体学、降雨分类、地震估计曲线、滑坡数据等方面分析断层结构和地表脆弱性格局和方向。粉砂岩地球化学特征是从断层构造区域外的选定岩石露头中收集的。在哈桑努丁大学地质系光学矿物实验室进行鉴定之前，在每个位置收集了粘土岩、砂岩和粉砂岩样品。断层应力结构的格局和走向以及粉砂岩地球化学特征影响了陆地的脆弱性。地震活动趋势与区域尺度断层高度相关，如几内亚褶皱逆冲断层带、格蒂尔-鲁法尔中央山脉断层、萨米断层、战网断层、曼贝拉莫断层等。影响局部尺度断层区南部的地震动力学与具有剪切面的剥落岩石区重叠。有交替的砂岩、灰岩、粘土岩和粉砂岩层，其化学成分为铝、钙、铁、钾和镁，以及岩层的年龄。剪切面脆弱性可能导致土壤侵蚀和不稳定的边坡。根据测绘结果，在昂格雷索东北部、先锋比拉克以北和卡索纳韦亚西南部发现了脆弱性极高的地区。此外，在缅甸南部的山坡上也发现了高脆弱性区

Received: March 26, 2021 / Revised: April 24, 2021 / Accepted: May 25, 2021 / Published: June 28, 2021
About the author: Adi Tonggiroh, Department of Geology, Hasanuddin University, Makassar, Indonesia
Corresponding author Adi Tonggiroh, adi.tonngiroh19@gmail.com

域，而卡诺纳韦贾和缅甸的土地脆弱性被归类为中或低。露头的存在和具有剪切面的剥落岩石对研究区粉砂岩结构对土地敏感性的影响很大。

关键词：断层应力结构，土地，脆弱性，地球化学特征，曼巴莫开斋节。

1. Introduction

Mamberamo Raya is one of the districts in Papua, Indonesia. This region is part of the Papua geological feature formed by the convergent motion between Australia and the Pacific plates [1]. Convergent motion is accommodated by thrusting in the Highlands and Mamberamo thrust belt. This region has experienced frequent powerful earthquakes, which may cause tsunamis and landslides. Data indicated that every earthquake event was associated with numerous active faults in the land of Papua and the surrounding area. One of these active faults is located in Mamberamo Raya [2]. This situation leads the site prone to disaster. Based on the statistical data, several high-magnitude earthquakes occurred in this region: 8.1 in 1916, 8.1 in 1971, 7.8 in 1990, and 4.0–7.2 in 2010–2016. In 2019, landslide incidents accompanied by flash floods were recorded in Sentani District, Jayapura Province. That occurred because of high rainfall of 248.5 mm a day, Cyclops faults, and earthquake frequency of 3.3–5.4 RS two months before the incident. Similar situations are also suspected in Mamberamo Raya because of frequent rainfalls and earthquakes. In addition, the vulnerability of the area to disasters is also affected by its existing faults and rock formations. Chemical processes in rocks may affect landslides because of the stone weathering process. This effect increases in areas with alternating layers of sandstone, greywacke, claystone, and siltstone. Chemical weathering mechanisms weaken the engineering properties of sandstones and conglomerates [3].

The convergence motion of the two plates is generally followed by collisions caused by the interaction of movements between island arcs and continental plates, which occurred during the Cenozoic Era [4]. The impact of the interaction is closely related to the regional geological structures that cross the northern and southern parts, namely, (1) the fold and thrust fault belt of Guinea, (2) the fracture of the Central Gauttier–Roufaer Mountains, (3) the Mamberamo fault and (4) the Waropen fault [5].

In the form of fractures and folds, signs of rock deformation began to appear from various types of rock dip [5], [6]. Steep slope due to morphological cuts and changes in the type of river trellis correlates with physical silt sediment, marl, clay, sandstone, and conglomerate. Those are weathered rock types indicating changes like chemical physics [7]. In this region, the stone characteristics' changes following the weathering processes are never uniform in terms of depth. Thus, it became a weak zone acting as a slip plane, which leads to landslide incidents [8]. In tropical climates [9], high rainfall triggers landslides [10]. It exerts a hydrochemical effect of evapotranspiration, soil moisture, and reduced cohesiveness by weathering on rocks with carbonate composition [11]. Finally, the release of rock particles on a slope variation affects landslide susceptibility.

Land vulnerability is identified as a quantitative or qualitative assessment of the classification, volume (or area), spatial distribution of erosion, soil displacement, or landslides, which exist or might occur in an area [6]. Previous studies on land vulnerability identified that landslides might be caused by topographical, geological, geomorphological, and geotechnical properties, climate, vegetation, and anthropogenic factors, with the distribution of past events [6], [12]. A study about geological factors, including rock types, also revealed that volcaniclastics trigger coseismic landslides. Shales and sandstones are most often associated with landslides, where the latter being mostly associated with disturbed landslides [6], [13]. Other research showed the relationship between morphological, lithological, and geomorphological conditions and rainfall events that trigger mass movements, such as falling rocks, landslides, and rapid earth flows [14]. However, a more detailed atrocity of siltstone geochemistry characteristics and its relationship with land vulnerability has not received considerable attention.

Development activities of the government certainly require research support so that the direction of regional development can meet the engineering requirements, including geological aspects. Some regional development programs lack consideration of geological aspects. An example is the construction of the Regent Office Building of Mamberamo on the fault plane. Although there have been numerous research libraries on landslides, no research is conducted in the area dominated by the Mamberamo formation consisting of siltstone, sandstone, and claystone. This study aimed to analyze the relationship of the pattern and direction of the fault–stress structure and geochemical characteristics of siltstone to land vulnerability.

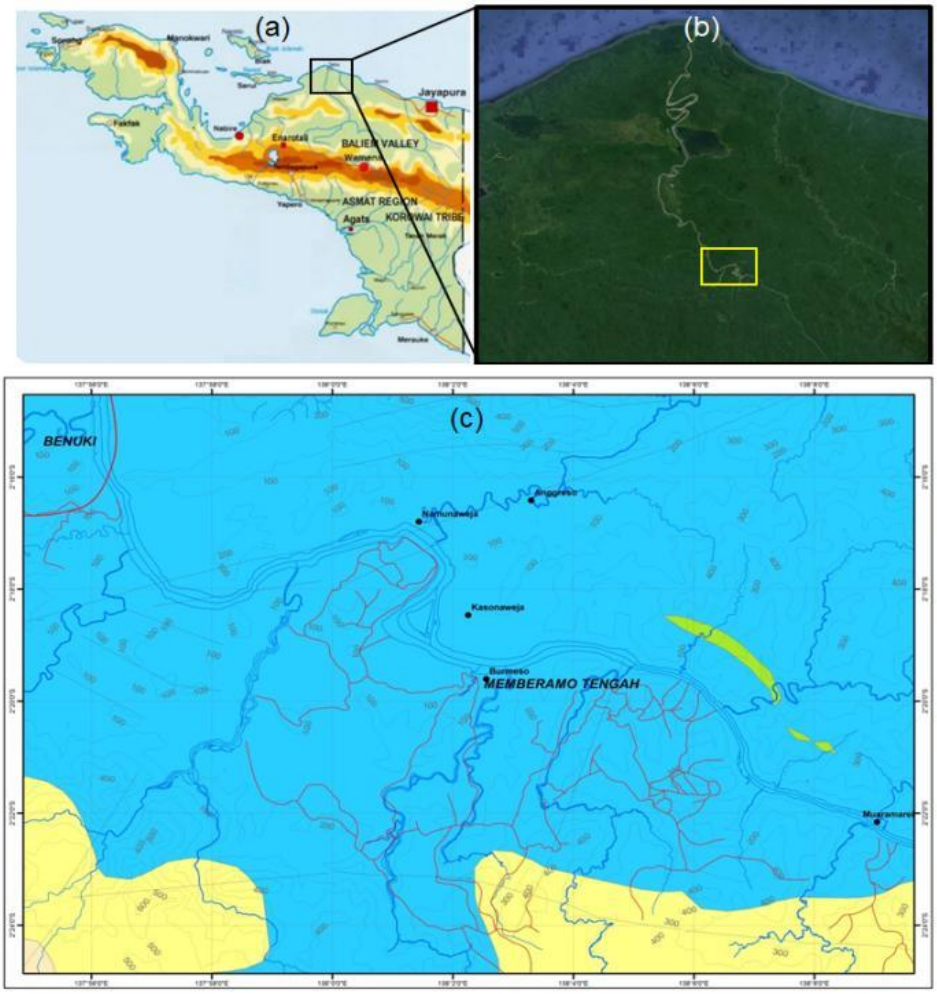

Fig.1 Map of study site: (a) Papua region, (b) study site, (c) location of the study site

2. Material and Methods

2.1. Location Characteristics

The study was conducted in Burmeso dan Kasonaweja sub-districts of Mamberamo, about 238 km southwest of Jayapura, the capital city of Papua province. The Mamberamo is located between Sarmi and Waropen Districts (Figure 1).

2.2. Data Collection

Data were collected from field and secondary sources, such as the digital map and the Meteorology, Climatology, and Geophysical Agency. Field surveys were conducted in 21 stations. Four out of 21 stations were selected as representative areas for observation and collection of rock outcrops, petrographic and geochemical characteristics of siltstone. In each location, claystone, sandstone, and siltstone samples were collected before their identification in the Laboratory of Optical Minerals at the Department of Geology, Hasanuddin University. Tests on siltstone outcrop were conducted using hydrochloric acid to induce a carbonic acid reaction since siltstone reacts with acidic solutions.

2.3. Data Analysis

The pattern and direction of the fault–stress structure, slope, earthquake, and land vulnerability were analyzed from the direct interpretation of the Digital Elevation Model (DEM) using Landsat map image version 8. Rainfall data from 2010 to 2018 were obtained from meteorological stations maintained by the Meteorology, Climatology, and Geophysical Agency, Jayapura. Earthquake data were acquired from Station 5 in Papua province, covering the Mamberamo Raya, Mamberamo Tengah, Barnes, and Dabra areas.

The data analysis was done by interpreting DEM map alignment, outcrop description, petrography, stereographic geological structures, rainfall classification, and earthquake estimation curves. Then, the correlation between earthquake scale and depth was analyzed using quadratic correlation. The multi-dynamic effect is very complicated regarding the rock and geological structure phases in the study area; the fault can be reactivated many times if the area is affected by various phases of deformation.

Four siltstone samples were prepared in quartile forms, which were then analyzed via X-ray fluorescence spectrometry at the Geochemical Laboratory of the Department of Geological Engineering, Hasanuddin University. The 146 earthquake data were sorted into 102 based on the

magnitude range (1–9.5 on the Richter scale) and depth range (1–1000 km). The results of the petrographic analysis, structural geological affirmation, slope, and earthquake data from the spatial layer overlay were integrated to understand and determine the relationship between geological structures and landslide triggers description of outcrops, petrography, and stereology of geological structures.

3. Results and Discussions

Stratigraphy is generally composed of two object rock formations based on regional geological maps. First is the Unk formation in the Pliocene–Pleistocene era, composed of sandstones, siltstones, and coal inserts. This formation consists of stones belong to members B, C, D, and E classes and stored in fluvial, delta, and bathyal environments. Member C consists of conglomerate sequence, sandstone (sub-greywacke sandstone), siltstone, and shale; Member D consists of the alternates between Member C and Member D; Member E consists of conglomerate, sandstone, siltstone, shale, and lignite. Second is the Makats formation, composed of conglomerate rocks, sandstones, siltstone, and shale. The Mamberamo formation is composed of sedimentary rocks formed in fluvial, delta, and bathyal environments. This characteristic is observed in siltstones containing fossils.

3.1. Structure Geological Characteristics and Earthquake

Measurement of the muscular and shear orientation along the river path and morphological intersections revealed a strong correlation of dynamic motions between faults and folds. The lineament results were used to understand the geological complexity of the study site based on the outcrop study and the earthquake hazard zonation. Trellis and dendritic flow patterns were very common and characterized by brecciation, mylonite, and gouge. This pattern was known as induction of sinistral faults and anticline folds trending northwest-southeast to east-west that were relatively unidirectional, with a regional fault Yapen EW or WNW-ESE [15]. This formation indicated a relationship between the Sarmi fault and the Mamberamo fault.

Solid analysis on siltstone in the Burmeso area has three directions, namely, (1) N 50° E and N 40° W, with the available sturdy position being northeast; (2) N 20° W and N 70° E, with the available sturdy position being northeast-southwest; and (3) N 60° W and N 30° E, with the available sturdy position being southwest–northwest. This three-way affirmation altered the siltstone layer, which initially had an average angle of <20° then increased to 35°–65°. It was suspected to be a trigger for landslides. Further analysis revealed a continuous trend of the landslide distribution following a dominant change to the northwest.

The solid analysis of siltstone and sandstone interlayer in the Kasonaweja area revealed two general directions of stress, (1) N N E and (2) N 50° W; N 40° E. These two strings also increased the dip of the rock bed, which initially had an average angle of <23° to 100°–170°. The field data demonstrated that the fault zone might transform siltstone into incompressible, mylonite, and gouge. Moreover, the landslide distribution in the form of a spot did not continuously follow the dominant dip changes toward the southwest and the cohesiveness of the rock layers (Figures 2a, 2b). The intertwining of siltstone and sandstone layers was two types of rocks when mutual interaction formed shifts along the bedding field.

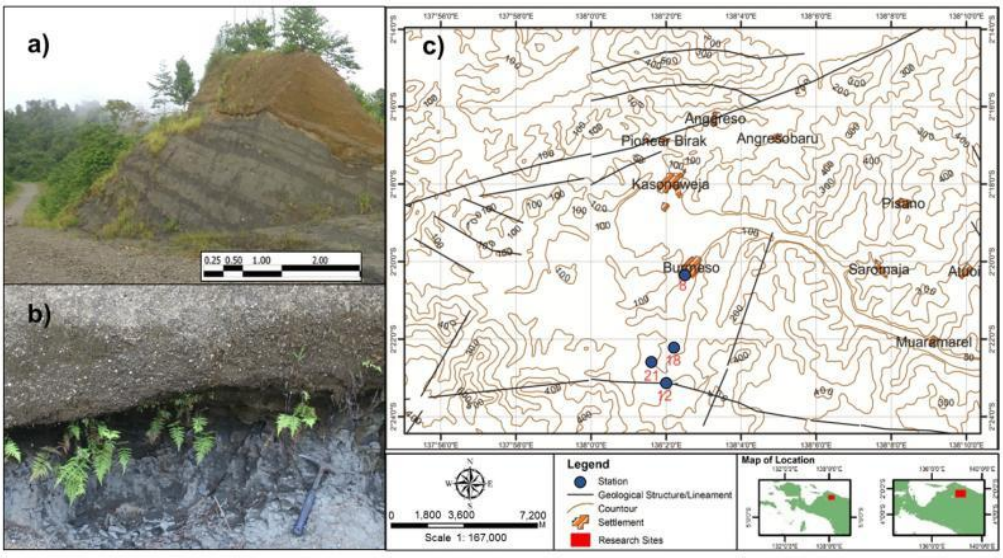

Fig. 2 Siltstone and sandstone strips in a side of the outcrop (a), the physical characteristic of siltstone (b), geological structure in the study site (c)

The geological structure of the study area was complicated by the measurement of the direction of affirmation on the distribution of siltstone and sandstone. Stereographic analysis of four points (ST 8, 12, 18, 21), as follows: (1) σ1 (118° / 70°), σ2 (298° / 19°), σ3 (28° / 7°) was siltstone (2) σ1 (107° / 69°), σ2

(289° / 21°), σ3 (19° / 5°) was sandstone (3) σ1 (86° / 66°), σ2 (251° / 21°), σ3 (348° / 13°) was siltstone (4) σ1 (110°) / 69°), σ2 (302° / 21°), σ3 (34° / 3°) was siltstone (Figure 3). The stereographic projection analysis result showed the direction of the maximum main stress of the study area tended to be in the southeast direction with the minimum main stress trending north-east (NE), except Station 18 that is northeast (NE) with the direction of the main strength of the minimum trending northwest (NW). Therefore, the main stress tended to project to the southeast–north to northeast–west direction. The main stress differences determined by the fan diagram analysis method and stereographic projection indicate that the force held in the Mamberamo Raya Regency area is continuous, which causes a reflection of the Yapen regional fault forming faults afterward. This result can be proven by the number of topographical (linear) lineages in this area.

The formation of geological structures occurs. First, there is a compression force in the Unk formation in the northwest-southeast and southwest-northeast directions, causing anticline folds.

The faults significantly trigger geological disasters, such as landslides. Moreover, broken rocks weather easily, crumble, and accelerate the process of landslides. Since the faults occur in soft rocks in the investigation area, they are easily destroyed and cause landslides. Avalanches in the investigation area generally occur in rocks with low specific resistance. The direction of the landslide plane usually follows the direction of the rock layers. The landslide is strongly influenced by the activity of the geological structures in the area under investigation. The landslide slip plane relatively follows the direction of the fracture plane slope of the rock. Based on the results of the measurements of the fracture in the field with an angle of inclination of 25°–30°, it can be inferred that the landslide field always follows the fracture plane.

As indicated by the mapping results, earthquakes repeatedly occur at the same source point (epicenter). It is more likely to be associated with the fold and thrust fault belt of Guinea, Gauttier fault, Roufaer fault, and Appauwer fault, which affected the local-scale fault. Further analysis demonstrated that the largest earthquake distribution is in the southeastern part of the study area. Therefore, the most vulnerable land to earthquakes was found in that area (Figure 4).

Statistical analysis of 102 earthquake data (2010–2018) revealed the following: magnitude distribution on a range of 4.0–6.0 Richter scale; skewness, −0.1 and 0.72; and kurtosis, 0.143 or 0.481 $-2 < x < 2$.

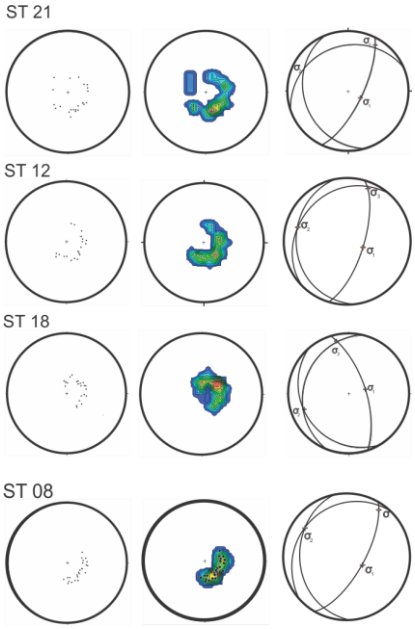

Fig. 3 Results of joint analysis using stereography-9 projection

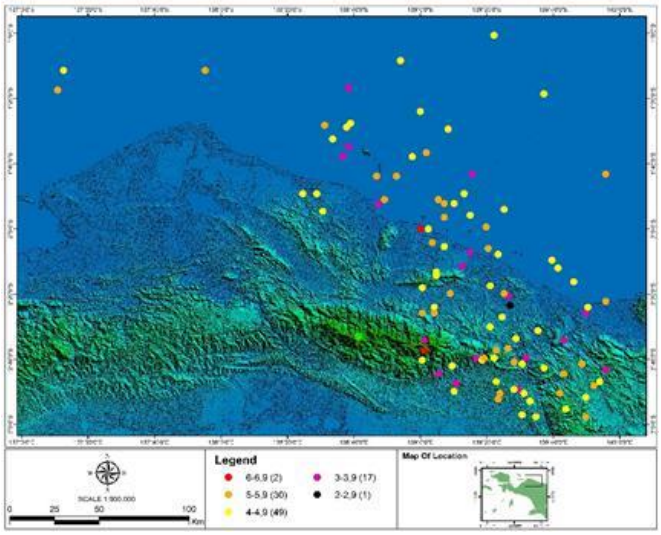

Fig. 4 The magnitude and distribution of earthquakes in Mamberamo from 2010 to 2016

The tendency of positive skewness demonstrates the even and repeated distribution of earthquake points. In comparison, negative skewness showed the correlation of earthquake source with the regional motion from Guinea's fold and thrust fault belt, Gauttier fault, Roufaer fault, and Appauwer fault. Pearson's correlation coefficient is as follows: magnitude, −0.99; depth, 1.0. It indicates that earthquakes correlate with active regional-scale faults that exert a domino effect on local-scale faults. This finding is consistent with the continuity of the fault line that intersects the Marine Valen Rapids and numerous government buildings, such as the Mamberamo District Office. Their effects were known from friction records of silt crushed by shifting the dip-slip fault plane (Figure 5b).

This situation indicated that the Mamberamo geological structures contributed to earthquake events and caused land vulnerability in this area. Earthquakes

systematically affect rock stress, hill slopes, and erosion, causing cracks and fractures on mountain crests and flanks, promoting an increased frequency of landslides [16], [17].

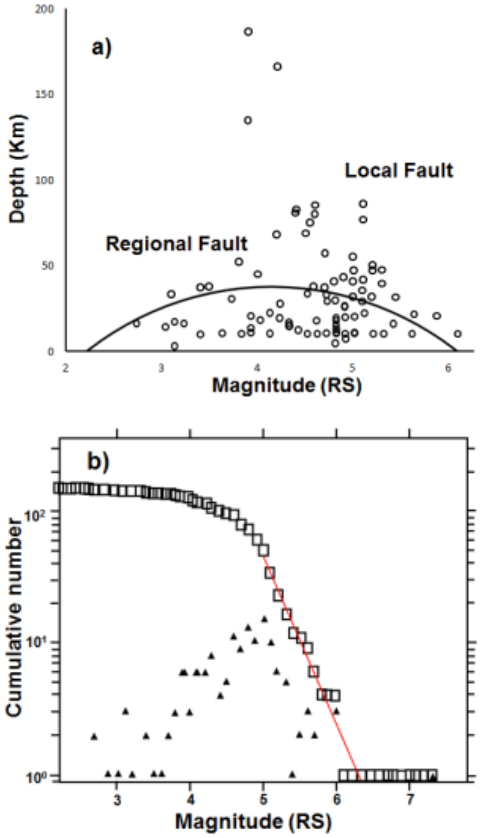

Fig. 5 The normal quadratic distribution of earthquake in Mamberamo: (a) Magnitude; (b) Frequency

3.2. Identification of Rock Outcrops

Description of the outcrops in the intercalation of the sandstones and siltstone 20° N, 10° E to 203° N,19° E, changed in the direction of the layer were characteristic of the formation of morphological blocks due to fracture. A detailed description of the physical changes and mineralogy using petrographic methods is presented in Figure 5. The results revealed that the rocks at the research location are dominated by sandy clay mixed with gravel. The characteristics of these rocks are described as follows:

a) Claystone: microscopically thin incision of sediment rock, orange absorption, black–gray interference, clastic texture, grain size <0.02 mm, angular–subangular-shaped grain, packed with good sorting. It composes of clay minerals (75%), muscovite (10%), biotite (10%), and quartz (5%);

b) Sandstone: microscopically thin incision of sediment rock, orange absorption, black–gray interference, clastic texture, grain size < 0.02–0.4 mm, angular–subangular-shaped mineral, closed containers with good sorting. Mineral composition consists of orthoclase (35%), quartz (5%), muscovite (20%), biotite (20%), plagioclase (10%), and clay minerals (10%);

c) Siltstone: macroscopically gray to brownish, macrofossils in the form of shellfish and other marine organisms, microscopically thin incision of siltstone, clay mineral matrix, and carbonate (90%), feldspar, quartz, and lithic (10%). Feldspar, quartz, and lithographic subangular-rounded grains were distinguished from quartz cement by a thin, fine layer around the grains. Magnetite and hematite exist as small grains (<0.01 mm) in the interparticle region. Rock mineral components are (matrix, 60%) oxide medium silt (0.01–0.03), carbonate (matrix, 30%), feldspar (subangular–poorly rounded 5%), lithic (3%, measuring < 0.1 mm), and opaque minerals (2%). Grain gradation separated by a thin layer of clay indicated that siltstone had a wide range of physical changes and disturbance of geological structure mechanisms. It also showed the dominance of carbonate composition ($CaCO_3$) (Figure 6).

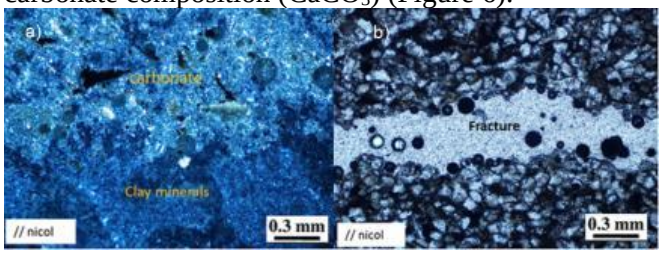

Fig. 6 The gradation of siltstone (a) and sandstone fracture (b)

The distribution of the elements Al, Ca, Fe, K, and Mg was closely associated with the chemical weathering properties of the claystone outcrops. These elements may combine with oxygen to form mineral fractions such as quartz (SiO_2), orthoclase ($KAlSi_3O_8$), albite ($NaAlSiO_8$), magnetite (Fe_3O_4), biotite ($KMgFe_3AlSi_3O_{10}FOH_2$), and muscovite ($KAl_2AlSi_3O_{10}FOH_2$). The presence of these minerals determines the nature of the rock. Claystones are generally located as an insert between siltstone and sandstone. This study found the presence of the mineral quartz in claystone. Quartz is classified as a resistant mineral to weathering. The presence of this mineral in claystone indicates partial weathering, which spreads horizontally in the siltstone and sandstone. Muscovite and biotite have a prismatic crystal cleavage structure, which easily turns into very thin sheets under pressure. This sheet spreads between the grains and further reduces the adhesive properties of siltstone, claystone, and sandstone. The fractional dynamic motion pressure of muscovite and biotite is a factor that weakens the physical properties of siltstone, claystone, and sandstone.

Siltstone composes several important mineral elements such as Fe, Ca, Al, Mg, and K, where high Fe, Ca, and Al are substantial elements for siltstone weathering (Figure 7). Pearson's negative correlation between Ca and Al (−0.676) indicates that only Ca has a different chemical reaction to Al in the weathering process.

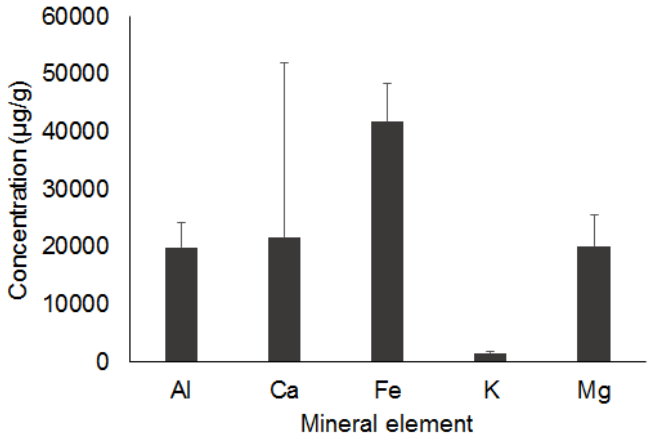

Fig. 7 Composition of siltstone constituent elements (mean ± SD)

Statistical analysis revealed the geochemical correlation of the alkaline elements Al, Ca, Fe, K, and Mg on the acidity index of rainwater to form hydroxide (OH) compounds. This result showed that vertical rainwater infiltration encourages weathering of siltstone. Under dry conditions, the siltstone outcrops in the field have two weathering features that cause the rock to become brittle: (1) the release of clay chemical bonds to the rock mineral components, and (2) when the rock becomes brittle, the quartz crystal grains fill the cavity of the clay mineral. Siltstone granules, consisting of rock components, quartz, opaque, carbonate, and feldspar, are bound by montmorillonite minerals. Under dry conditions, the crystal structure of montmorillonite minerals weakens due to the release of the Na–Ca cation bonds by water and hydroxyl infiltration.

3.3. Morphology and Landslide

Based on the field survey, the morphology of the study area was divided into two forms. First, the hilly shape was sliced sharply by a steep slope observed in the Saromaja and Pisano–Kasonaweja areas. Second, the jagged mountains were observed in the Anggreso Baru and Trimuris areas. However, these two morphologies were quite difficult to distinguish due to the influence of the geological structure and landslide activity, which changes the degree of the slope. The classification indicated that the slope was accompanied by subsidence; thus, the acceleration of the material movement on the surface was highly dependent on rainfall. Most landslides are caused by episodic events, such as heavy rainfall or events, earthquakes, or a combination of both [16], [18].

As for the tropical climate, the irregular rainfall shows its maximum range in November–May (404.0–841.8 mm) and the minimum range in June–October (44.6–170.0 mm) (Figure 8). The maximum range and minimum range difference are considered quite significant due to water infiltration in the soil pore. The rock swells lead to vertical deformation [19]. The deformation structures in the sliding surface consisted of fault scarps and folds. These structures are interpreted in terms of basal shear stresses formed during the avalanche. Three major joint sets were identified at the sliding surface. The clay mineral expansion occurred in siltstone, claystone, and sandstone. Since nine years' data revealed a high mean annual rainfall (2841 mm), this level was considered high risk as data revealed that landslides most likely occur in numerous areas with an annual rainfall ≥ 2500 mm per year [20], [21].

The physical change occurs in the fault plane where mylonite rock collapses are formed, shear fractures, and folded structure wings. On the surface, especially along the exposed outcrop, erosion is developed in the siltstone layer, a physical property of easy destruction. Due to heavy rain, erosion triggers landslides, reduces slope stability, and causes vulnerable hillsides to coseismic landslides [22]. Underneath the soil layer, strips of sandstones and siltstones can be found. Both stones easily interact to form a slip along with the layer [23]. The contact layer forms a 20° planar slope, which, along with the geological structure of the 25°–30° planar slope, reduces the cohesiveness and triggers landslides. Fracture morphology control is held in the Middle East Mamberamo, Mamberamo Hulu and Roufaer, west and southeast Mamberamo, Burmeso, Kasonaweja with the general direction of north–northwest–south–southeast, and southwest-northeast [24].

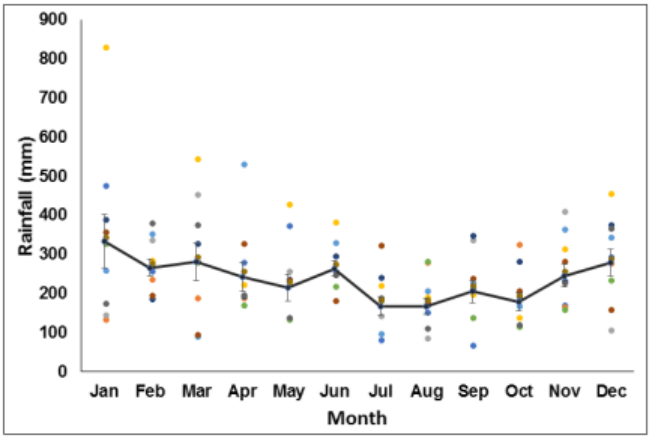

Fig. 8 Rainfall fluctuation from 2010 to 2018

The correlation of fault, morphology, and siltstone observed is characterized by changes in the siltstone layer position [25]. It sometimes occurs at the top of the sandstone layer and vice versa. When the siltstone layer is at the top, especially at fractures and morphological junctions, this condition facilitates rain absorption and triggers landslides.

The land vulnerability map (Figure 9) illustrates a very high-level risk in the northeast of Anggreso, north of Pioneer Birak, and partly southwest of Kasonaweja. In addition, high vulnerability is also seen on the hillside, south of Burmeso. Meanwhile, in Kanonaweja

and Burmeso, land vulnerability is classified as medium or low. The highly vulnerable land in the north, northeast, and south is caused by faults and fractures, while lithological factors cause soil vulnerability.

The implication of this research shows that several vulnerable areas cross the vital settlement area and event government office building, for example, the regent's office. Due to the high level of vulnerability in the area, this study recommends relocating the vital office building. However, this would have several constraints, including budgeting and political instability. Therefore, in the short term, efforts to strengthen the early warning system are urgently needed.

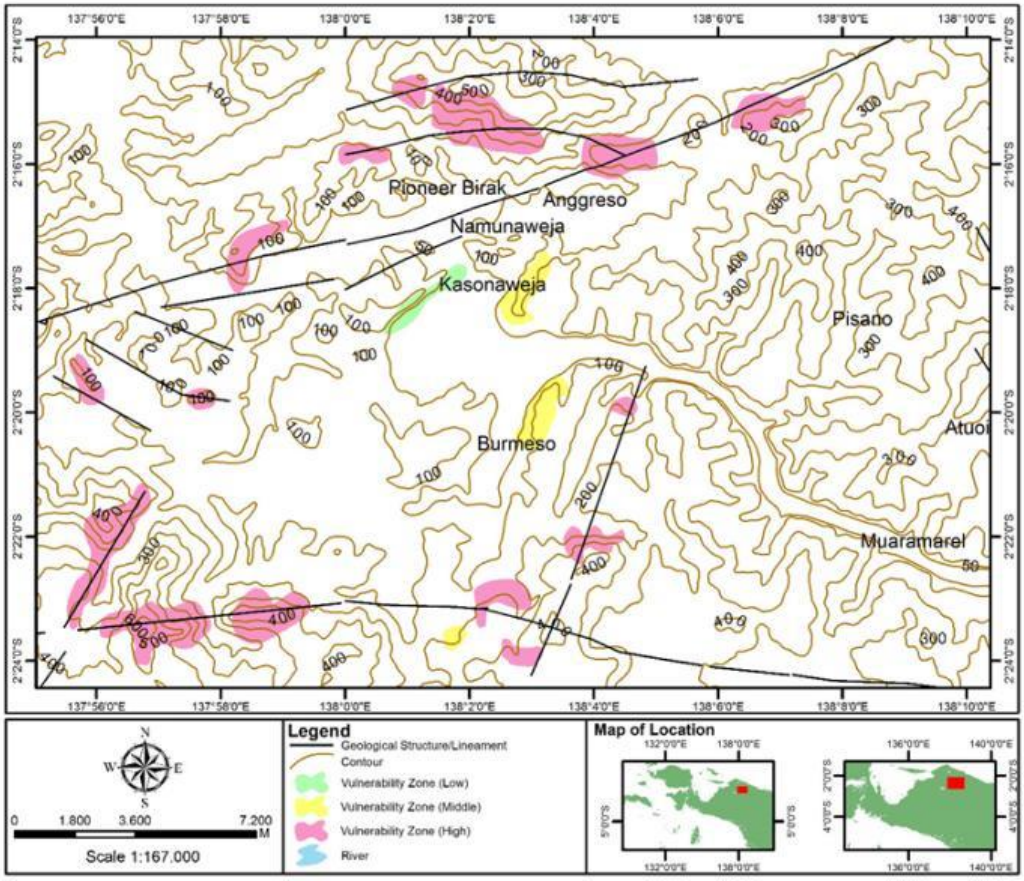

Fig. 9 Land vulnerability map in the study area in Mamberamo

4. Conclusion

The pattern and direction of the fault–stress structure and the geochemical characteristics of siltstone affect land vulnerability. The observations of rock outcrops revealed an overlapping rock layer composed of claystone, which is considered an insertion between siltstone and sandstone. Since the stone composes of Ca, Fe, Al, and Si, it indicates the vulnerability to chemical weathering. It easily reacts with rainwater, thus accelerating land vulnerability, erosion, and unstable slopes. Based on the mapping results, the areas with high vulnerability are located in the northeast of Anggreso, north of Pioneer Birak, and part of the southwest of Kasonaweja. Additionally, high vulnerability is also detected on the hillside south of Burmeso, while in Kanonaweja and Burmeso, land vulnerability is classified as medium or low.

5. Suggestion

Further study is needed to describe the larger-scale structure and the main faults in the Regional Geology of Mamberamo and analyze the impacts of the earthquake on the landslide.

Acknowledgement

The author thanks Mamberamo Regency Government, Papua Province. Thanks to Eply L.S. Sembor, Muktiadi Mahmud, Herry A. Iwanggin, Edwin S. Maker, Yan Ibo, Yohanis Rumbiak, Leonard Rumansa, for assisting field sampling.

References

[1] MAMENGKO D. V., SENDJADJA Y. B., and MULYANA B. Perkembangan Fasies Sedimen Formasi Mamberamo Berumur Miosen Akhir-Pliosen di Cekungan Papua Utara. *Jurnal Geologi dan Sumberdaya Mineral*, 2019, 20(1): 37-47. http://dx.doi.org/10.33332/jgsm.geologi.v20i1.399

[2] SIANIPAR D. S. J., & SERHALAWAN Y. R. Pemodelan Mekanisme Sumber Gempa Bumi Ransiki 2012 Berkekuatan Mw 6, 7. *Jurnal Sains dan Teknologi*, 2017, 6(1); 148-157. http://dx.doi.org/10.23887/jst-undiksha.v6i1.9333

[3] IÑIGO A. C., GARCÍA-TALEGÓN J. A., and VICENTE-PALACIOS V. Measuring the Effectiveness and Durability of Silicified Sandstones and Conglomerates from Zamora, Spain Subject to Silico-organic Treatments and/or Freezing/Thawing Processes. *Rock Mechanics and Rock Engineering*, 2021. https://doi.org/10.1007/s00603-021-02434-x

[4] VAN HINSBERGEN D. J. J., STEINBERGER B., and DOUBROVINE P. V. Acceleration and Deceleration of India-Asia Convergence since the Cretaceous: Roles of Mantle Plumes and Continental Collision. *Journal of Geophysical Research*, 2011, 116: 1-20. https://doi.org/10.1029/2010JB008051

[5] BABAULT J., MUZAS M. V., and LEGRAND X. Source-to-Sink Constraints on Tectonic and Sedimentary Evolution of the Western Central Range and Cenderawasih Bay (Indonesia). *Journal of Asian Earth Sciences*, 2018, 156: 256-287. https://doi.org/10.1016/j.jseaes

[6] MARSALA V., GALLI A., and PAGLIA G. Landslide Susceptibility Assessment of Mauritius Island (Indian Ocean). *Geosciences*, 2019, 9: 1-26. https://doi.org/10.3390/geosciences9120493

[7] HADI A. I., BROTOPUSPITO K. S., and PRAMUMIJOYO. Regional Landslide Potential Mapping in Earthquake-Prone Areas of Kepahiang Regency, Bengkulu Province, Indonesia. *Geosciences*, 2018, 8: 1-16. https://doi.org/10.3390/geosciences8060219

[8] LAZZARI M., & PICCARRETA M. Landslide Disasters Triggered by Extreme Rainfall Events: the Case of Montescaglioso (Basilicata, Southern Italy). *Geosciences*, 2018, 8: 1-17. https://doi.org/10.3390/geosciences8100377

[9] LI X., WU H., and QIAN H. Groundwater Chemistry Regulated by Hydrochemical Processes and Geological structures: A Case Study in Tongchuan, China. *Water*, 2018, 10: 1-16. https://doi.org/10.3390/w10030338

[10] BURBERRY C. M., SWIATLOWSKI J. L., and SEARLS M. L. Joint and Lineament Patterns across the Midcontinent Indicate Repeated Reactivation of Basement-Involved Faults. *Geosciences (Switzerland)*, 2018, 8: 1-24. https://doi.org/10.3390/geosciences8060215

[11] ROMERO-MUJALLI G., HARTMANN J., and BÖRKER J. Ecosystem Controlled Soil-Rock pCO2 and Carbonate Weathering – Constraints by Temperature and Soil Water Content. Chemical Geology, 2018, 527: 1-11. https://doi.org/10.1016/j.chemgeo.2018.01.030.

[12] SALVATI P., BIANCHI C., ROSSI M., and GUZZETTI F. Societal Landslide and Flood Risk in Italy. Natural Hazards Earth System Sciences, 2010, 10, 465-483. https://doi.org/10.5194/nhess-10-465-2010

[13] LATO M., BOBROWSKY P., ROBERTS N., BEAN S., POWELL S., MCDOUGALL S., BRIDEAU M.-A., STEAD D., and VANDINE D. Site investigation, analysis, monitoring and treatment, Canadian technical guidelines and best practices related to landslides: a national initiative for loss reduction. *Geological Survey of Canada, Open File 8114*. Natural Resources Canada, 2016. https://doi.org/10.4095/299117

[14] CHUNGA K., LIVIO F. A., and MARTILLO C. Landslides Triggered by the 2016 mw 7.8 Pedernales, Ecuador earthquake: Correlations with ESI-07 Intensity, Lithology, Slope and PGA-h. *Geosciences*, 2019, 9: 1-16. https://doi.org/10.3390/geosciences9090371

[15] LIU F., LI J., and YANG S. Landslide Erosion Associated with the Wenchuan Earthquake in the Minjiang River Watershed: Implication for Landscape Evolution of the Longmen Shan, Eastern Tibetan Plateau. *Natural Hazards*, 2015, 76: 1911-1926. https://doi.org/10.1007/s11069-014-1575-8

[16] FAN X., SCARINGI G., and KORUP O. Earthquake-Induced Chains of Geologic Hazards: Patterns, Mechanisms, and Impacts. *Reviews of Geophysics*, 2019, 57: 421-503. https://doi.org/10.1029/2018RG000626

[17] MARC O., BEHLING R., and ANDERMANN C. Long-Term Erosion of the Nepal Himalayas by Bedrock landsliding: the role of monsoons, earthquakes and giant Landslides. *Earth Surface Dynamic*, 2019, 7: 107-128. https://doi.org/10.5194/esurf-7-107-2019

[18] DOU J., YUNUS A. P., and BUI T. D. Evaluating GIS-Based Multiple Statistical Models and Data Mining for Earthquake and Rainfall-Induced Landslide Susceptibility Using the LiDAR DEM. *Remote Sensing*, 2019, 11*:* 638. https://doi.org/10.3390/rs11060638.

[19] SCHULZ W. H., SMITH J. B., WANG, and GONGHUI. Clayey Landslide Initiation and Acceleration Strongly Modulated by Soil Swelling. *Geophysical Research Letters*, 2017, 45: 1888-1896. https://doi.org/10.1002/2017GL076807

[20] CHEN C.-W., SAITO H., and OGUCHI T. Rainfall Intensity–Duration Conditions for Mass Movements in Taiwan. *Progress in Earth and Planetary Science*, 2015, 2: 1-14. https://doi.org/10.1186/s40645-015-0049-2

[21] GUTIÉRREZ-MARTÍN A., HERRADA M. Á., and YENES J. I. Development and Validation of the Terrain Stability Model for Assessing Landslide Instability During Heavy Rain Infiltration. *Natural Hazards Earth Systematic Science*, 2019, 19: 721-736. https://doi.org/10.5194/nhess-19-721-2019

[22] SAITO H., UCHIYAMA S., and HAYAKAWA Y. S. Landslides Triggered by an Earthquake and Heavy Rainfalls at Aso Volcano, Japan, Detected by UAS and SfM-MVS Photogrammetry. *Progress in Earth and Planetary Science*, 2018, 5: 1-10. https://doi.org/10.1186/s40645-018-0169-6

[23] RASO E., CEVASCO A., and DI MARTIRE D. Landslide-Inventory of the Cinque Terre National Park (Italy) and Quantitative Interaction with the Trail Network. *Journal of Maps*, 2019, 15(2): 818-830, https://doi.org/10.1080/17445647.2019.1657511

[24] TONGGIROH A., JAYA A. H. S., and IRFAN U. R. Geological Study and Regional Development of Mamberamo Raya District of Papua Province, Indonesia. *Journal of Physics: Conference Series*, 2018, 962: 1-8. https://doi.org/10.1088/1742-6596/962/1/012023

[25] LI G., WEST A. J, and DENSMORE A. L. Seismic Mountain Building: Landslides Associated 20with the 2008 Wenchuan Earthquake in the Context of a Generalized Model for Earthquake Volume Balance. *Geochemistry, Geophysics, Geosystems*, 2014, 15: 833-844. https://doi.org/10.1002/2013GC005067

参考文:

[1] MAMENGKO D. V., SENDJADJA Y. B., 和 MULYANA B. 北巴布亚盆地晚中新世-上新世曼贝拉莫

组沉积相的发育。地质矿产资源杂志, 2019, 20(1): 37-47. http://dx.doi.org/10.33332/jgsm.geologi.v20i1.399
[2] SIANIPAR D. S. J., 和 SERHALAWAN Y. R. 模拟 2012 年兰西基地震震级为 6、7 的震源机制. 科技学报, *2017*, 6(1); 148-157. http://dx.doi.org/10.23887/jst-undiksha.v6i1.9333
[3] IÑIGO A. C., GARCÍA-TALEGÓN J. A., 和 VICENTE-PALACIOS V. 测量来自西班牙萨莫拉的硅化砂岩和砾岩经过有机硅处理和/或冷冻/解冻过程的有效性和耐用性。岩石力学与岩石工程, 2021. https://doi.org/10.1007/s00603-021-02434-x
[4] VAN HINSBERGEN D. J. J., STEINBERGER B., 和 DOUBROVINE P. V. 白垩纪以来印亚辐合的加速和减速：地幔柱和大陆碰撞的作用。地球物理研究杂志, 2011, 116: 1-20. https://doi.org/10.1029/2010JB008051
[5] BABAULT J., MUZAS M. V., 和 LEGRAND X. 中西部山脉和仙德拉瓦西湾（印度尼西亚）构造和沉积演化的源汇约束。亚洲地球科学杂志, 2018, 156: 256-287. https://doi.org/10.1016/j.jseaes
[6] MARSALA V., GALLI A., 和 PAGLIA G. 毛里求斯岛（印度洋）滑坡敏感性评估。地球科学, 2019, 9: 1-26. https://doi.org/10.3390/geosciences9120493
[7] HADI A. I., BROTOPUSPITO K. S., 和 PRAMUMIJOYO. 印度尼西亚明古鲁省克帕香克帕香摄政地震多发区的区域滑坡潜力绘图。地球科学, 2018, 8: 1-16. https://doi.org/10.3390/geosciences8060219
[8] LAZZARI M., 和 PICCARRETA M. 极端降雨事件引发的山体滑坡灾害：以蒙泰斯卡廖索（意大利南部巴西利卡塔）为例。地球科学, 2018, 8: 1-17. https://doi.org/10.3390/geosciences8100377
[9] LI X., WU H., 和 QIAN H. 受水化学过程和地质结构调控的地下水化学：以中国铜川为例。水, 2018, 10: 1-16. https://doi.org/10.3390/w10030338
[10] BURBERRY C. M., SWIATLOWSKI J. L., 和 SEARLS M. L. 横跨中部大陆的节理和线状模式表明涉及基底的断层反复激活。地球科学（瑞士）, 2018, 8: 1-24. https://doi.org/10.3390/geosciences8060215
[11] ROMERO-MUJALLI G., HARTMANN J., 和 BÖRKER J. 生态系统控制的土壤-岩石二氧化碳分压和碳酸盐风化——受温度和土壤含水量的限制。化学地质, 2018, 527: 1-11. https://doi.org/10.1016/j.chemgeo.2018.01.030.
[12] SALVATI P., BIANCHI C., ROSSI M., 和 GUZZETTI F. 意大利的社会滑坡和洪水风险。自然灾害地球系统科学, 2010, 10, 465-483. https://doi.org/10.5194/nhess-10-465-2010
[13] LATO M., BOBROWSKY P., ROBERTS N., BEAN S., POWELL S., MCDOUGALL S., BRIDEAU M.-A., STEAD D., 和 VANDINE D. 现场调查、分析、监测和处理、加拿大技术指南和与滑坡相关的最佳实践：减少损失的国家倡议。加拿大地质调查局，打开文件 8114。加拿大自然资源部, 2016. https://doi.org/10.4095/299117
[14] CHUNGA K., LIVIO F. A., 和 MARTILLO C. 2016 年厄瓜多尔佩德纳莱斯地震引发的山体滑坡：与环境地震烈度表强度、岩性、坡度和峰值地面加速度的相关性。地球科学, 2019, 9: 1-16. https://doi.org/10.3390/geosciences9090371
[15] LIU F., LI J., 和 YANG S. 岷江流域汶川地震滑坡侵蚀对青藏高原东部龙门山景观演变的启示.自然灾害, 2015, 76: 1911-1926. https://doi.org/10.1007/s11069-014-1575-8
[16] FAN X., SCARINGI G., 和 KORUP O. 地震引发的地质灾害链：模式、机制和影响。地球物理学评论, 2019, 57: 421-503. https://doi.org/10.1029/2018RG000626
[17] MARC O., BEHLING R., 和 ANDERMANN C. 基岩滑坡对尼泊尔喜马拉雅山的长期侵蚀：季风、地震和巨型滑坡的作用。地表动态, 2019, 7: 107-128. https://doi.org/10.5194/esurf-7-107-2019
[18] DOU J., YUNUS A. P., 和 BUI T. D. 使用光检测测距数字高程模型评估基于地理信息系统的多个统计模型和数据挖掘地震和降雨诱发的滑坡敏感性.遥感, 2019, *11*: 638. https://doi.org/10.3390/rs11060638.
[19] SCHULZ W. H., SMITH J. B., WANG, 和 GONGHUI. 土壤膨胀强烈调节粘土滑坡的发生和加速。地球物理研究快报, 2017, 45: 1888-1896. https://doi.org/10.1002/2017GL076807
[20] CHEN C.-W., SAITO H., 和 OGUCHI T. 台湾群众运动的降雨强度-持续时间条件。地球与行星科学进展, 2015, 2: 1-14. https://doi.org/10.1186/s40645-015-0049-2
[21] GUTIÉRREZ-MARTÍN A., HERRADA M. Á., 和 YENES J. I. 用于评估暴雨下渗期间滑坡不稳定性的地形稳定性模型的开发和验证。自然灾害地球系统科学, 2019, 19: 721-736. https://doi.org/10.5194/nhess-19-721-2019
[22] SAITO H., UCHIYAMA S., 和 HAYAKAWA Y. S. 由日本阿苏火山地震和暴雨引发的滑坡，由无人机系统和运动中的结构 - 多视图立体摄影测量检测到. 地球与行星科学进展, 2018, 5: 1-10. https://doi.org/10.1186/s40645-018-0169-6
[23] RASO E., CEVASCO A., 和 DI MARTIRE D. 五渔村国家公园（意大利）的滑坡清单和与步道网络的定量相互作用。地图杂志, 2019, 15(2): 818-830, https://doi.org/10.1080/17445647.2019.1657511
[24] TONGGIROH A., JAYA A. H. S., 和 IRFAN U. R. 印度尼西亚巴布亚省曼巴莫开斋节区的地质研究和区域发展。物理学杂志：会议系列, 2018, 962: 1-8. https://doi.org/10.1088/1742-6596/962/1/012023
[25] LI G., WEST A. J, 和 DENSMORE A. L. 地震山体建筑：在地震体积平衡的广义模型背景下与 20 与 2008 年汶川地震相关的滑坡。地球化学、地球物理学、地球系统, 2014, 15: 833-844. https://doi.org/10.1002/2013GC005067